STRUCTURAL CONTROL AND HEALTH MONITORING
*Struct. Control Health Monit.* 2012; **19**:535–547
Published online 23 March 2011 in Wiley Online Library (wileyonlinelibrary.com). DOI: 10.1002/stc.452

# ARX residuals in damage detection

Dionisio Bernal[1,*,†], Daniele Zonta[2] and Matteo Pozzi[2]

[1]*Northeastern University, Civil and Environmental Engineering Department, Center for Digital Signal Processing, Boston, MA 02115, U.S.A.*
[2]*University of Trento, DIMS, via Mesiano 77, 38050 Trento, Italy*

## SUMMARY

The relationship between residuals obtained from Autoregressive with Exogenous Input (ARX) predictors is examined from the perspective of resolution in damage detection. It is shown that residuals from all ARX structures are filtered versions of those obtained when only inputs are used to compute the predictions, i.e. the output error (OE) residuals. Examination shows that the transfer matrix from the OE residuals to the equation error (EE) ones has repeated poles at the origin and transmission zeros and zero directions that coincide with the poles and eigenvectors of the input–output map. This result, together with an examination of the spectral distribution of the OE residuals suggest that these are likely more informative for damage detection than the EE ones. Results of a Monte Carlo study and tests on an aluminum beam, where damage is simulated by the addition of a small mass, are shown to support this contention. Copyright © 2011 John Wiley & Sons, Ltd.

Received 9 April 2010; Revised 12 November 2010; Accepted 29 January 2011

KEY WORDS: damage detection; ARX; ARMAX; residuals; structural health monitoring

## 1. INTRODUCTION

This paper considers the residual approach to damage detection and examines, specifically, how selection of output error (OE) or equation error (EE) residuals from Autoregressive with Exogenous Inputs (ARX) models [1,2] affects resolution. We recall, for clarity, that the term EE is used to indicate that the reference signals are obtained using inputs and measured outputs, while OE indicates that only the reference model and the measured inputs are used. The result that is central to the paper and which supports the discussions throughout is a derivation showing that the EE residuals are the convolution of the OE ones with a kernel defined by the coefficient matrices of the autoregressive part of the ARX model. More specifically, the derivation shows that the poles of the reference model (whether these are physical or not) are transmission zeros of the transfer matrix relating the OE to the EE residuals and that the associated zero directions coincide with the eigenvectors.

Work explicitly focused on investigating the relation between OE and EE residuals from ARX predictors is not known to the writers, but related research on data-driven fault detection schemes is extensive. The classical approach, introduced by Mehra and Peschon [3], takes the residuals as the innovations of a Kalman filter [4] and uses deviations from anticipated whiteness to announce damage [3,5]. The innovation correlations scheme is particularly

*Correspondence to: Dionisio Bernal, Northeastern University, Civil and Environmental Engineering Department, Center for Digital Signal Processing, Boston, MA 02115, U.S.A.
†E-mail: bernal@neu.edu

attractive when the statistics of the process and measurement noise are stable throughout the monitoring period, but it is less so when this is not the case because the filter reacts to all changes and it is necessary to distinguish between changes in the noise statistics from changes in the system. Investigations that have used ARX residuals to detect damage include the one by Peeters [6], the related works by Lu and Gao [7] and Gao and Lu [8] and the AR-ARX scheme presented by Shon and Farrar [9].

On the identification of the ARX model parameters from the data there are many excellent references; we note the classic texts by Ljung [1], Soderstrum and Stoica [2], and the more recent one by Verhaegen and Verdult [10]. Albeit not based on the ARX structure, a residual-based detector that has received much attention in the structural health monitoring community uses differences from the product of two matrices that are orthogonal under the null hypothesis (i.e. that the system is not damaged). One of the matrices is the left kernel of an observability block identified from data of the reference state and the other is a Hankel matrix of covariance functions from the interrogation phase. Details of this approach can be found in [11–13]. General reviews on fault detection, including discussion of the residual based strategy, can be found in Baseville [14], Willsky [15], Frank [16], Patton *et al.* [17] and Fassois [18] among others. Finally, on the important issue of the effect of environmental changes on damage detection, the reader is referred to the recent review given by qSohn [19].

This paper begins with some observations on the extraction of the reference ARX model from measurements and continues with the analytical examination of the connection between the OE and EE residuals. Examination on how damage affects the spectrum of the OE residuals and a brief discussion on the selection of a damage discriminating metric conclude the analytical part of the paper. The numerical section contains a Monte Carlo study and results from an experiment where damage in an aluminum beam is simulated by the addition of a small mass. A concluding section with a review of the main points closes the paper.

## 2. THE REFERENCE MODEL

Two strategies can be used to account for the existence of process and measurement noise when a model for the deterministic input–output relation is desired, namely: (1) the disturbances and measurement noise can be accommodated by over-specifying the order of the deterministic input–output or, (2) an explicit noise model can be included in the parameterization. In the first case one obtains an estimate of the deterministic input–output by removing modes that appear related to the noise [20]. In the numerical analyzes in this paper the ARX models are obtained by fitting an Autoregressive Moving Average with Exogenous input (ARMAX) [1,2] to the data and then removing the MA part. The general ARMAX model is

$$\sum_{j=0}^{n_\alpha} \alpha_j\, y(k-j) + \sum_{j=0}^{n_\beta} \beta_j u(k-j) + \sum_{j=0}^{n_e} \gamma_j\, e(k-j) = 0 \tag{1}$$

where $\alpha_j$, $\beta_j$ and $\gamma_j$ are coefficient matrices, $n_\alpha$, $n_\beta$ and $n_e$ are the orders of the autoregressive exogenous and moving average parts, $y$ is the measured output vector, $u$ is the deterministic input vector and $e$ is white noise. In the general ARMAX model the orders noted are independent but in structural applications it is common to operate under the premise that the analog input is of the form $u(\tau) = f_0(\tau)u(k) + f_1(\tau)u(k+1)$, where $\tau$ is at the origin of each time step and $f_0(\tau)$ and $f_1(\tau)$ are time invariant functions [21]. For this condition it has been shown that the three orders can be taken as equal [22] so one can write the ARX model as

$$\sum_{j=0}^{n} \alpha_j\, y(k-j) + \sum_{j=0}^{n} \beta_j u(k-j) = 0 \tag{2}$$



DOI: 10.1002/stc

## 3. RESIDUAL GENERATION

### 3.1. EE

Using Equation (2) to solve for $y(k)$ as a function of past values (i.e. taking $\alpha_0 = -I$) one has

$$\hat{y}_M(k) = \sum_{j=1}^{n} \alpha_j \, y(k-j) + \sum_{j=0}^{n} \beta_j u(k-j) \tag{3}$$

where the hat notation indicates a computed quantity (as opposed to a measured one) and the subscript $M$ indicates that the estimate is affected by the output measurements. The EE residual is, therefore,

$$\varepsilon_{EE}(k) = y(k) - \hat{y}_M(k) = y(k) - \sum_{j=1}^{n} \alpha_j \, y(k-j) - \sum_{j=0}^{n} \beta_j u(k-j) \tag{4}$$

or, more compactly

$$\varepsilon_{EE}(k) = -\sum_{j=0}^{n} \alpha_j \, y(k-j) - \sum_{j=0}^{n} \beta_j u(k-j) \tag{5}$$

### 3.2. OE

The OE residuals are the difference between the measurements and the predictions obtained using only the input. The pure simulation prediction can be computed from the weighting sequence description [23] (i.e. from convolution of the appropriate pulse response with the input) or, more conveniently for our purpose, by replacing the measured output with the model prediction in the ARX structure, namely

$$\hat{y}_O(k) = -\sum_{j=1}^{n} \alpha_j \, \hat{y}_O(k-j) - \sum_{j=0}^{n} \beta_j u(k-j) \tag{6}$$

where the subscript 'O' has been added to distinguish the result from that in Equation (3). Subtracting the measurement at (k) from both sides of Equation (6) one gets

$$\varepsilon_{OE}(k) = y(k) - \sum_{j=1}^{n} \alpha_j \, \hat{y}_O(k-j) - \sum_{j=0}^{n} \beta_j u(k-j) \tag{7}$$

## 4. TIME DOMAIN RELATION BETWEEN OE AND EE RESIDUALS

Solving for the exogenous input term using Equation (7) and placing the result in Equation (5) one gets

$$\varepsilon_{EE}(k) = -\sum_{j=0}^{n} \alpha_j y(k-j) + \sum_{j=1}^{n} \alpha_j \hat{y}_O(k-j) - y(k) + \varepsilon_{OE}(k) \tag{8}$$

Recalling that $\alpha_0 = -I$ and that $\varepsilon_{OE}(k) = y(k) - \hat{y}_O(k)$ gives

$$\varepsilon_{EE}(k) = -\sum_{j=0}^{n} \alpha_j \varepsilon_{OE}(k-j) \tag{9}$$

which shows that the EE residuals are filtered versions of the OE ones, and that the kernel is the AR part of the model.

## 5. FREQUENCY DOMAIN RELATION BETWEEN OE AND EE RESIDUALS

Further insight into the relationship between the residuals can be developed from an examination in the $z$-domain. We recall for clarity that the $z$-transform on the unit circle, i.e.



DOI: 10.1002/stc

when $z = e^{-i\omega\Delta t}$, is the same as a discrete time Fourier Transform and that as the (positive) frequency goes from zero to Nyquist, $z$ moves from 1 to $-1$ along the upper half of the unit circle. To get the transfer matrix ($T(z)$) we take a $z$-transform of Equation (9) and get

$$\varepsilon_{EE}(z) = T(z)\varepsilon_{OE}(z) \tag{10}$$

where it is evident that

$$T(z) = -\sum_{j=0}^{n} \frac{\alpha_j}{z^j} \tag{11}$$

or

$$T(z) = -\frac{1}{z^n} \sum_{j=0}^{n} \alpha_j z^{n-j} \tag{12}$$

Equation (12) shows that the OE to EE transfer matrix has $n$ repeated poles at the origin and $n$ transmission zeros [24,25]. To illustrate the relation between transmission zeros and zero directions and the properties of the identified system we take a $z$-transform of Equation (2) and, solving for the output as a function of the input, get

$$y(z) = \left[\sum_{j=0}^{n} \alpha_j z^{n-j}\right]^{-1} \left[\sum_{j=0}^{n} \beta_j z^{n-j}\right] \{u(z)\} \tag{13}$$

Comparison of the matrix that is inverted in Equation (13) with the summation in Equation (12) shows that the two are identical so one concludes that the poles of the identified input–output map coincide with the transmission zeros of the OE to EE residual transfer matrix. Moreover, since $y(z)$ becomes parallel to the null space of the inverted matrix as $z$ approaches a pole it follows that the eigenvectors of the identified input–output coincide with the transmission zero directions.

### 5.1. The transfer function

In the single output case $T(z)$ becomes a scalar function and (since the $\alpha$'s in Equation (11) are scalars) one can write

$$T(z) = -\alpha_n \prod_{j=1}^{n} \left(\frac{1}{z} - \frac{1}{\bar{z}_j}\right) \tag{14}$$

or

$$T(z) = -\alpha_n \prod_{j=1}^{n} \left(\frac{\bar{z}_j - z}{\bar{z}_j z}\right) \tag{15}$$

where $\bar{z}_j$ is the $j$th identified pole. From Equation (12) one has

$$-z^n T(z) = \sum_{j=0}^{n} \alpha_j z^{n-j} \tag{16}$$

and, since the polynomial on the right side of Equation (16) is monic, its independent term is equal to the product of its roots (with a minus sign in this case because of the minus sign of $\alpha_0$), so one has

$$\alpha_n = -\prod_{j=1}^{n} \bar{z}_j \tag{17}$$

Substituting Equation (17) into Equation (15) gives

$$T(z) = \frac{1}{z^n} \prod_{j=1}^{n} (\bar{z}_j - z) \tag{18}$$

which is the general expression of the transfer function between OE and EE residuals.



DOI: 10.1002/stc

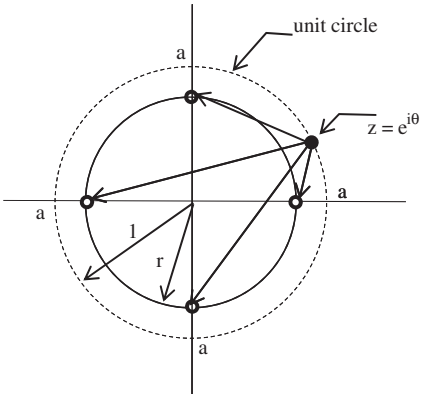


Figure 1. Geometric interpretation of the numerator of Equation (18).

*5.1.1. Uniformly spaced poles.* Insight into the qualitative behavior of the OE to EE transfer function can be gained by looking at Equation (18) in the idealized case where $n$ poles are uniformly spaced on a radius $r<1$. Since we consider the poles to be at constant radial distance and the magnitude of a pole in the $z$-domain is $|\bar{z}| = r = \mathrm{e}^{-\omega\xi\Delta t}$ it follows that we are considering the case where damping is inversely proportional to frequency. The situation is illustrated (for $n=4$) in Figure 1. From inspection of this figure and considerations of symmetry it is evident that the product on the *rhs* of Equation (18) is the same in each of the segments of the unit circle delimited by the intersection of radii passing through adjacent poles. In this simple case it is possible to derive a closed form expression for $T(z)$ as follows:

*Lemma*
Given $z = \mathrm{e}^{\mathrm{i}\theta}$ and $\bar{z}_j = r\mathrm{e}^{2\pi ki/n}$ $k = 0, 1, 2, \ldots n-1$, (where $n$ is even) one has

$$\prod_{j=0}^{n-1}(\bar{z}_j - z) = (\mathrm{e}^{\theta ni} - r^n) \tag{19}$$

*Proof*
From Figure 1 it is evident that

$$\prod_{j=0}^{n-1}(\bar{z}_j - z) = \prod_{j=0}^{n-1}\left(r\mathrm{e}^{\frac{2\pi j}{n}i} - \mathrm{e}^{\theta i}\right) \tag{20}$$

or

$$\prod_{j=0}^{n-1}(\bar{z}_j - z) = \prod_{j=0}^{n-1}\mathrm{e}^{\frac{2\pi j}{n}i}\left(r - \mathrm{e}^{\left(\theta - \frac{2\pi j}{n}\right)i}\right) \tag{21}$$

The product outside the parenthesis on the *rhs* equals minus one so one has

$$\prod_{j=0}^{n-1}(\bar{z}_j - z) = -\prod_{j=0}^{n-1}\left(r - \mathrm{e}^{\left(\theta - \frac{2\pi j}{n}\right)i}\right) \tag{22}$$

The second term on the *rhs* parenthesis are the $n$ roots of $-\mathrm{e}^{\theta ni}$ so it follows (recalling that the product of the roots of a monic polynomial is equal to the independent term) that the *rhs* in Equation (22) is the factorization of the monic polynomial $r^n - \mathrm{e}^{\theta ni}$. □

From the previous lemma and Equations (18) and (19) one finds that the OE to EE transfer function for the case of uniformly spaced poles is

$$T(z) = \frac{(\mathrm{e}^{n\theta i} - r^n)}{\mathrm{e}^{n\theta i}} \tag{23}$$

Inspection of Equation (23) shows that the amplitude of $T(z)$ fluctuates between $1-r^n$ to $1+r^n$ and the phase between $\phi = \pm\tan^{-1}(r^n)$. For sufficiently large $n$, therefore, the transfer



DOI: 10.1002/stc

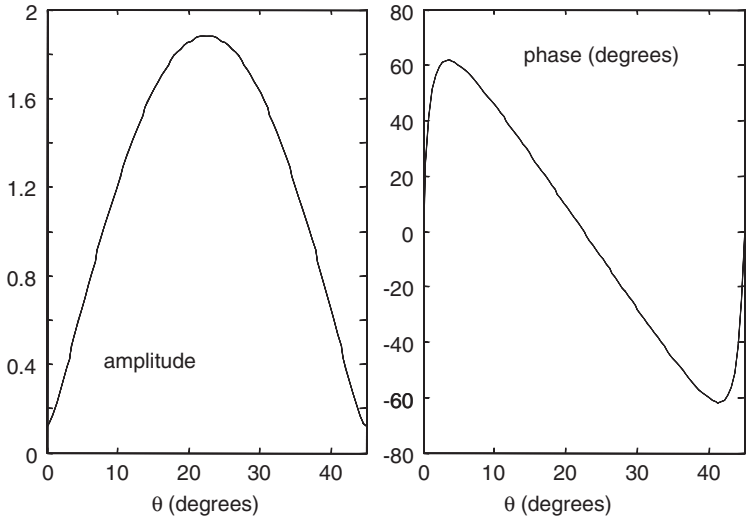


Figure 2. Transfer function between OE and EE residuals for a system or order eight with uniformly spaced poles located in the unit circle at a radius $r = 0.984$.

resembles an all-pass filter. For small $n$ values, however, the situation typically encountered in practice, $T(z)$ displays attenuation at the poles and amplification at the midpoint between poles. A Bode plot of $T(z)$ for 5% damping at a sampling to modal frequency of 20 is plotted in Figure 2 for $n = 8$. As can be seen, the attenuation at the poles in this case is 0.118 and the amplification between poles = 1.882. Although the result of Equation (23) is exact only in the case of uniformly spaced poles, the fact that $T(z)$ tends to attenuate the frequency components in the vicinity of the natural frequencies of the (reference and the damaged) system holds in general.

*5.1.2. Effect of the sampling frequency on the OE to EE transfer function*. The sampling frequency determines the position of the system poles on the unit circle and, as a consequence, has an important effect on $T(z)$. Specifically, for fast sampling the poles appear in the vicinity of $z = 1$ and, as one can see from Equation (18), the magnitude of $T(z)$ becomes large as $z$ approaches the Nyquist limit. Indeed, in the limiting case all the terms in the numerator of Equation (18) equal 2 and the magnitude of $T(z)$ at Nyquist reaches $2^n$. Explicitly stated, for fast sampling one anticipates that the EE residuals will have large high frequency noise because any noise contained in the OE residuals will be highly amplified. Consider, for example, a 4-DOF chain system with lumped masses equal to {1 2 1 3 } and stiffness values equal to 100 in some consistent set of units. Figure 3 plots, for the case of 2% damping in each mode, and a measurement at the 4th DOF, the magnitude of the transfer function from the OE to the EE residuals for two different sampling: $\Delta t = 0.15$ and 0.01 s. The large time step is such that the Nyquist frequency is close to the highest frequency mode and the fast represents, therefore, oversampling by a factor of nearly 15. As can be seen, $|T(z)|$ reaches very large values in the fast sampling case. The fact that the residuals when sampling is fast are dominated by the amplification of the high frequency noise is illustrated in Figure 4, which shows the OE and EE residuals when damage is modeled as 10% loss of stiffness in the first spring and the measurement is contaminated with additive noise having a standard deviation equal to 5% of the measurement.

## 6. DAMAGE RELATED CONTRIBUTIONS TO THE OE RESIDUALS

The filtering that takes place in passing from the OE to the EE residuals proves beneficial or detrimental for damage detection depending on how the damage contributions to the OE residuals are distributed in frequency. One can gain some insight into the damage-related OE



DOI: 10.1002/stc

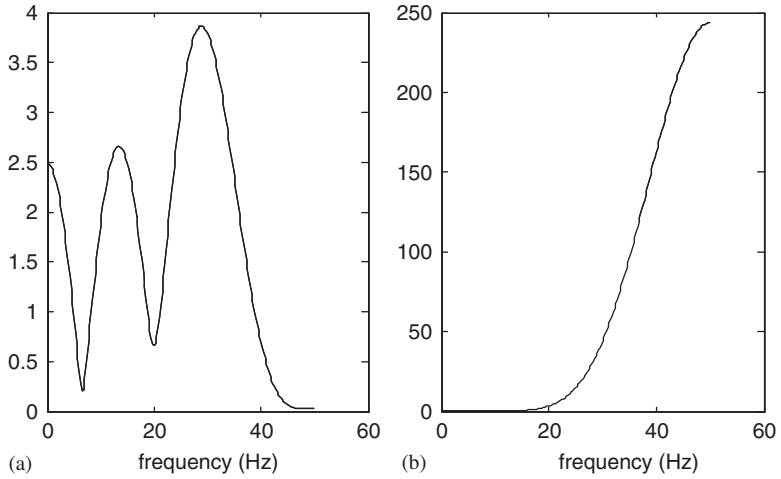


Figure 3. Amplitude of transfer function between OE and EE residuals for two sampling rates: (a) $\Delta t = 0.15$ s and (b) $\Delta t = 0.01$ s; the system is the 4-DOF system described in the text and the measurement is at the 4th DOF.

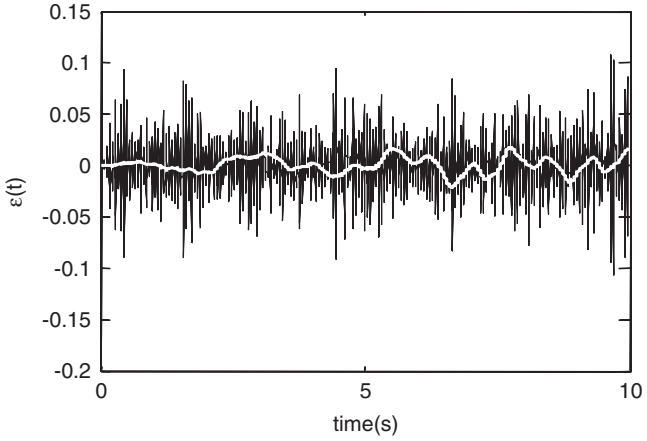


Figure 4. Time history of residuals for the 4-DOF described in text when damage is simulated as 10% loss of stiffness on spring ♯1; dark is EE and white is OE (units of $\varepsilon$ are fractions of g).

residual distribution as follows: using the superscript $u$ to refer to the undamaged, or reference state, and the superscript $d$ for the potentially damaged (or interrogation) stage one has, with $Y$ as the discrete time Markov parameters [23]

$$\hat{y}_{OE}(k) = \sum_{j=1}^{k} Y^u(k-j)u(j) \tag{24}$$

$$y^d(k) = \sum_{j=1}^{k} Y^d(k-j)(u(j)+\omega(j))+v(k) \tag{25}$$

where $\omega$ and $v$ are the unmeasured disturbances and the measurement noise. Recognizing that

$$\hat{y}_{OE}(k)+\varepsilon_{OE}(k) = y^d(k) \tag{26}$$

one gets, after some simple algebra

$$\varepsilon_{OE}(k) = v(k)+\sum_{j=1}^{k} Y^d(k-j)\omega(j)+\sum_{j=1}^{k} \Delta Y(k-j)u(j) \tag{27}$$



DOI: 10.1002/stc

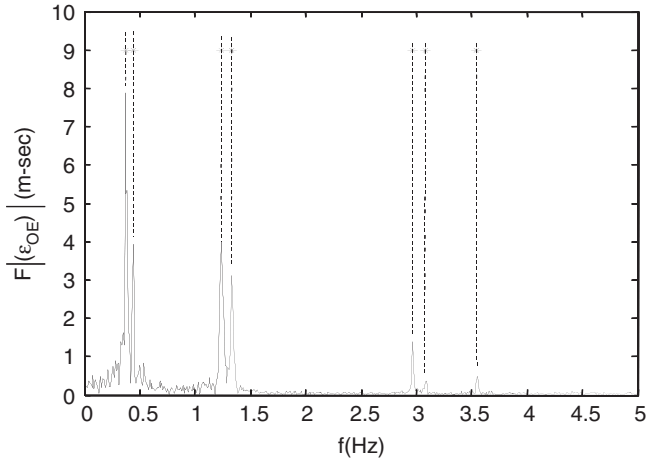


Figure 5. Spectrum of the OE residual at the 4th DOF for the 4-DOF system described in the text when the system is damaged (40% loss of stiffness on spring ♯1); the dotted lines are the location of the natural frequencies of the system in the undamaged and damaged states.

which shows that the OE residuals are the sum of three contributions. The first term is (assumed) white, the second is narrow band with peaks at the damaged state frequencies, and the third is the difference of the response in the damaged and the undamaged states to the deterministic input. This last term is narrow band and has peaks at the frequencies of the undamaged and of the damaged state. To verify the previous arguments we compute the amplitude of the Fourier spectrum of the OE residuals for the 4-DOF system considered in the previous example but increase the damage to 40% to make the separation of the frequencies between the undamaged and damaged state readily appreciated. The result depicted in Figure 5 is the average of 20 simulations with different realizations of the excitation and the noise. The fact that the spectrum of the OE residuals has peaks at the undamaged and damaged poles is evident from the figure. We note that the change in the frequency of the 4th mode is too small to be seen in the scale shown.

### *6.1. Anticipated effect of the OE to EE filtering on damage detection effectiveness*

Accepting that the model order is likely small (say less than 10 or so) and that significant oversampling is typical in practice, it can be stated that the dominant features of the OE to EE transfer are: (1) attenuation around the reference system poles and (2) amplification of the high frequency OE residuals. Since the damage-related contributions to the OE residuals concentrate in the region where the transfer function has a strong attenuation, one anticipates that the OE residuals will prove more informative for damage detection than the EE ones.

## 7. POWER OF DETECTION

To contrast the damage detection resolution of OE and EE residuals it is necessary to select a metric from the residual and to adopt a discriminating criterion. For the metric we use the ratio of the variance of the residual to the variance of the channel measurement, which in terms of signal norms can be expressed as

$$\chi = \frac{\|\varepsilon\|}{\|y_m\|} \tag{28}$$

where $\varepsilon$ is either $\varepsilon_{\mathrm{OE}}$ or $\varepsilon_{\mathrm{EE}}$ and the denominator is the measurement. Regarding the threshold for announcing damage we take it such that the probability of a false positive (Type I error) is no more than 5% and we judge relative performance in terms of the power of detection (POD), defined as one minus the probability of a false negative, i.e. one minus the probability of making



DOI: 10.1002/stc

an error of Type II. In the multi-output situation, the metric is computed for each channel and the decision logic is that if the result at any channel points to damage, then damage is announced.

## 8. MONTE CARLO STUDY

The system considered is depicted in Figure 6. Two sensor arrangements, seven damage distributions and three damage severities are examined. Only the single output case is considered. The sensor distributions are S1 = sensor in mass ♯3 and S2 = sensor in mass ♯5. The damage distributions are loss of stiffness in each one of the seven bars (one at a time) and damage severities are 2.5, 5, and 10% loss of stiffness. Two hundred simulations are carried out for each one of the 42 combinations considered. In each simulation the process noise is taken to be independent random signals acting on all masses with an RMS that, for each signal, is between 2 and 5% of the RMS of the deterministic excitation. The deterministic excitation in all cases is a wide band signal acting on mass ♯1. The measurement noise in each simulation has an RMS of 5% of the measured signal and damping is 2% in all modes.

The results are summarized in Figure 7. As anticipated by the analytical examination, the resolution of the OE residuals proves superior in all cases to that of the EE ones. In this case the

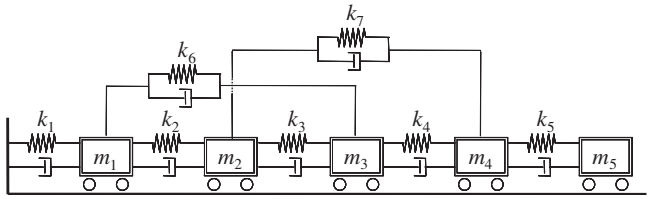


Figure 6. System used in the numerical study m1 ∼ m5 = 0.05, $k_1 = k_3 = k_5 = k_7 = 100$, $k_2 = k_4 = k_6 = 120$ (consistent units), damping is stiffness proportional with constant 0.002; the system's undamped natural frequencies are {2.6,7.2,13.3,14.7 and 16.5} Hz.

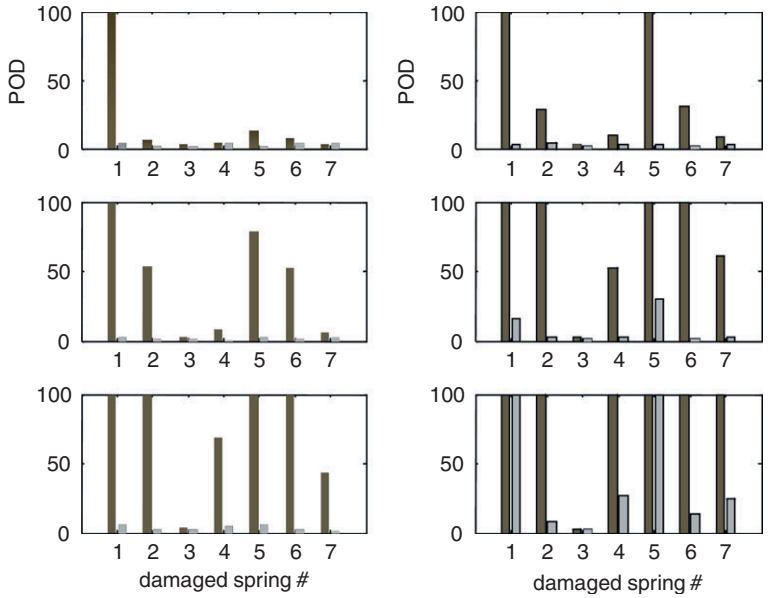


Figure 7. Power of detection at 5% type I error probability for the system of Figure 6; {a, b}, a = location of input, b = location of output. Left column in the figure {1,3 },right column {5,5} damage extent: top row in the figure 2.5%, middle row 5%, bottom row 10%; darker shade gives results from OE residuals and lighter shade from EE residuals.



DOI: 10.1002/stc

differences are large. For example, at the 10% stiffness loss level, the OE residuals provide close to 100% POD for all damaged patters while the EE residuals identify damage clearly only if it is on spring ♯1. Since our objective is to provide information on the contrast between the EE and OE residuals we do not expand the discussion on the performance of the OE residuals but note, however, that for the conditions considered here the OE residuals provide adequate damage detection (except for bar ♯3) at about 5% stiffness loss. The fact that damage in bar ♯3 proves difficult to identify is due to the fact that the equivalent pseudo-force provides little excitation in the lower modes, making this damage nearly unobservable.

## 9. EXPERIMENTAL INVESTIGATION

To further validate the analytically observations we examined an aluminum beam where damage was simulated by adding a small mass. The beam was tested in a free–free condition realized by hanging it from very flexible surgical tubing. A picture of the test setup showing the added mass in place and the suspension system is shown in Figure 8(a) with dimensions and other relevant numerical data depicted in Figure 8(b). As can be seen, the beam is excited by an electro-dynamic shaker and the response is recorded by five accelerometers located along the centerline axis. The force delivered by the shaker and the acceleration at the point of the force application were measured with an impedance head but acceleration at the shaker location was not used in the analysis. Three tests were carried out: the first one to formulate the reference ARX models, the second to compute the value of the metrics in and 'undamaged' case, and the third, with the added mass, to evaluate the metrics in the 'damaged condition'. Since data to estimate the probability distribution of the metric in the healthy state is not available, we do not attempt to estimate discriminating thresholds but simply report the metric relative sensitivity.

## 10. RESULTS

The analysis was first carried out on the premise that only one accelerometer was available at any given time. When formulating the model of the reference condition $n = 4$ (two pairs of complex modes) proved appropriate. Identified frequencies and damping ratios are summarized in Table I. As expected, the results from one sensor to the next are consistent, comparisons with analytical expressions showing that the identified frequencies correspond to the first two flexural modes. The values of the metric from Equation (28) are shown for all cases in Table II. Consistent with theoretical expectations, the sensitivity to 'the damage', relative to the change

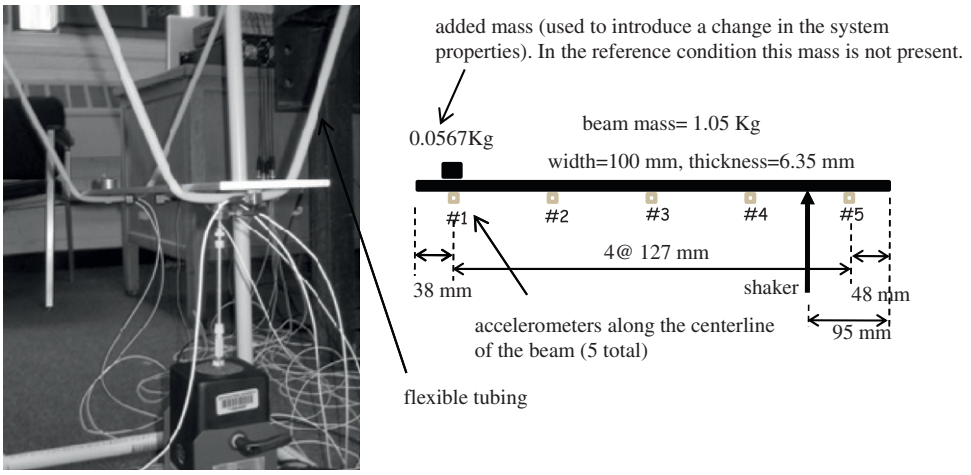


Figure 8. Free–free aluminum beam used in experimental examination.



DOI: 10.1002/stc

Table I. Identified frequencies and damping ratios in the formulation of the reference ARX models.

| Identification from channel | Mode #1 | | Mode #2 | |
|---|---|---|---|---|
| | Freq (Hz) | % damp | Freq (Hz) | % damp |
| 1 | 90.92 | 0.46 | 251.58 | 0.12 |
| 2 | 90.90 | 0.51 | 251.58 | 0.12 |
| 3 | 90.97 | 0.44 | 251.17 | 0.12 |
| 4 | 90.89 | 0.51 | 251.55 | 0.12 |
| 5 | 91.19 | 0.58 | 251.48 | 0.11 |
| 1–5 | 90.94 | 0.45 | 251.56 | 0.12 |

Table II. Results of experiments on the free–free aluminum beam (single output).

| Channel considered | Reference state | | Damaged state (added mass) | | Relative sensitivity | |
|---|---|---|---|---|---|---|
| | $\chi_{OE}$ | $\chi_{EE}$ | $\chi_{OE}$ | $\chi_{EE}$ | C3/C1 | C4/C2 |
| 1 | 0.0196 | 0.2144 | 3.0746 | 0.1329 | 156.87 | 0.62 |
| 2 | 0.0336 | 0.3866 | 1.9386 | 0.5924 | 57.70 | 1.53 |
| 3 | 0.4805 | 5.1903 | 0.4939 | 5.9390 | 1.03 | 1.14 |
| 4 | 0.0274 | 0.3065 | 1.7294 | 0.5338 | 63.12 | 1.74 |
| 5 | 0.2607 | 2.6281 | 1.4420 | 4.2012 | 5.53 | 1.60 |

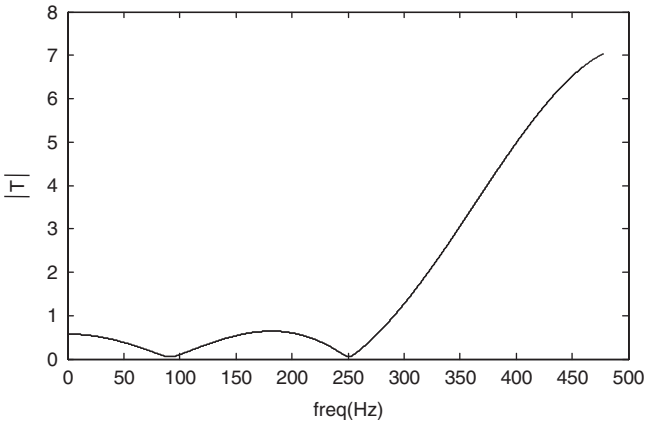


Figure 9. Amplitude of the residual transfer function for the model identified for the aluminum beam when the output sensor is #5.

between two undamaged cases, is much larger in the OE residuals than in the EE ones. Neither metric is sensitive to 'the damage' when the model is based on the output from sensor #3 and analysis shows that this is due to the fact that this sensor is very near the node of the first mode. For illustrative purposes Figure 9 depicts the amplitude of the residual transfer function for the case of sensor #5. Attenuation near the identified frequencies and amplification of the out-of-band components is evident.

In a final examination we looked at all the channels simultaneously. The frequencies obtained in this case are shown in the last row of Table I and, as one anticipates, are consistent with the results obtained in the single output cases. The channel-by-channel ratio of the metric in the damage and the healthy state for OE and EE are presented in Table III. As expected, the OE residuals prove significantly more sensitive to the damage than the EE ones.



DOI: 10.1002/stc

Table III. Results of experiments on the free–free aluminum beam (multi-output processing).

| | Relative sensitivity | |
|---|---|---|
| Computed at channel # | Ratio of $\chi_{OE}$ damaged to undamaged | Ratio of $\chi_{EE}$ damaged to undamaged |
| 1 | 184.2 | 4.3 |
| 2 | 67.6 | 1.9 |
| 3 | 1.8 | 8.2 |
| 4 | 110.7 | 1.8 |
| 5 | 12.5 | 2.0 |

## 11. CONCLUSIONS

Examination of the relationship between OE and EE residuals from ARX models shows that the later are filtered versions of the former. In the typical situation of low-order identification models, the basic features of the OE to EE filtering are attenuation of the contributions around the poles of the reference system and amplification of the high frequency components due to oversampling. Since most of the information on the OE residuals is concentrated in the vicinity of the system poles (for the undamaged and damaged states), the filtering to EE residuals typically has a detrimental effect in damage detection resolution. Results from simulations and from an experimental test were found in agreement with this contention.

## ACKNOWLEDGEMENTS

The first author acknowledges the support received from the University of Trento, Italy, where part of the study reported here was performed.

## REFERENCES

1. Ljung L. *System Identification*: *Theory for the User*. Prentice-Hal PTR: Upper Saddle River, NJ, 1999.
2. Soderstrom T, Stoica P. *System Identification*. Prentice Hall: Englewood Cliffs, NJ, 1989.
3. Mehra RK, Peschon J. An innovations approach to fault detection in dynamic systems. *Automatica* 1971; **7**:637–640.
4. Kalman RE. A new approach to linear filtering and prediction problems. *Journal of Basic Engineering* 1960; **82**:34–45.
5. Wright C, Bernal D. The Kalman filter whiteness test in damage detection: difficulties from variability in the noise statistics, *Proceedings IMACXXVI*, Jacksonville, FL, 2010.
6. Peeters B. System identification and damage detection in civil engineering, *Ph.D. Dissertation*, Katholieke Universiteit, Leuven, Belgium, 2000.
7. Lu Y, Gao F. A novel time-domain autoregressive model for structural damage diagnosis. *Journal of Sound and Vibration* 2005; **283**:1031–1049.
8. Gao F, Lu Y. A Kalman-filter based time-domain analysis for structural damage diagnosis with noisy signals. *Journal of Sound and Vibration* 2006; **297**:916–930.
9. Sohn H, Farrar CR. Damage diagnosis using time series analysis of vibration signals. *Smart Materials and Structures* 2001; (10):46–451.
10. Verhaegen M, Verdult V. *Filtering and System Identification*: *A Least Square Approach*. Cambridge University Press: Cambridge, 2007.
11. Basseville M, Abdelghani M, Benveniste A. Subspace-based fault detection algorithms for vibration monitoring. *Automatica* 2000; **36**:101–109.
12. Mevel L, Benveniste M, Baseville M, Goursant M. In operation structural damage detection and diagnosis. *COST F3*, Madrid, 2000.
13. Basseville M, Mevel L, Goursat M. Statistical model-based damage detection and localization: subspace-based residuals and damage-to-noise sensitivity ratios. *Journal of Sound and Vibration* 2004; **275**(3–5):769–794.
14. Basseville M. Detecting changes in signals and systems: a survey. *Automatica* 1988; **24**:309–326.
15. Willsky AS, Jones HL. A generalized likelihood ratio approach to the detection and estimation of jumps in linear systems. *IEEE Transactions on Automatic Control* 1976; **21**:108–112.
16. Frank PM. Fault diagnosis in dynamic systems using analytical and knowledge based redundancy—a survey and some new results. *Automatica* 1990; **26**(3):459–474.
17. Patton R, Frank PM, Clark N (eds). *Issues of Fault Diagnosis for Dynamic Systems*. Springer: Berlin, 2000.



DOI: 10.1002/stc

18. Fassois SD, Sakellarious JS. Time series methods for fault detection and identification in vibrating structures. *Proceedings of the Royal Society of London Transactions A* **365**:411–448.
19. Sohn H. Effects of environmental and operational on structural health monitoring. *Proceedings of the Royal Society of London Transactions A* 2007; **365**:539–560.
20. Pappa RS, Elliott KB, Schenk A. Consistent-mode indicator for the eigensystem realization algorithm. *Journal of Guidance, Control, and Dynamics* 1993; **16**(5):852–858.
21. Bernal D. Optimal discrete to continuous transfer for band limited inputs. *Journal of Engineering Mechanics* 2007; **133**(12):1370–1377.
22. Andersen P. Identification of civil engineering structures using ARMA models. *Ph.D. Thesis*, Department of Building Technology and Structural Engineering, Aalborg University, Denmark, 1997.
23. Juang JJ. *Applied System Identification*. Prentice Hall PTR: Upper Saddle River, NJ, 1994.
24. Antsaklis PJ, Mitchel AN. *Linear Systems*. Birkhäuser: Boston, MA, 2006.
25. Zhou K. *Essentials of Robust Control*. Prentice-Hall: Upper Saddle River, NJ, 1998.



DOI: 10.1002/stc